Quantifying Climate Feedbacks using Radiative Kernels

Brian J. Soden

Rosenstiel School for Marine and Atmospheric Science

University of Miami

Isaac M. Held

Geophysical Fluid Dynamics Laboratory

National Oceanic and Atmospheric Administration

Robert Colman

Bureau of Meteorology Research Centre

Melbourne, Australia

Karen M. Shell*, Jeffrey T. Kiehl, Christine A. Shields

National Center for Atmospheric Research

Boulder, CO

*Now at *Oregon State University*

Accepted *Journal of Climate*

Corresponding author: Dr. Brian J. Soden, Rosenstiel School for Marine and Atmospheric Science, University of Miami, 4600 Rickenbacker Cswy., Miami FL 33149.

Tel: (305) 421-4202, Fax: (305) 361-4457, email: bsoden@rsmas.miami.edu

Abstract

The extent to which the climate will change due to an external forcing depends largely on radiative feedbacks, which act to amplify or damp the surface temperature response. There are a variety of issues that complicate the analysis of radiative feedbacks in global climate models, resulting in some confusion regarding their strengths and distributions. In this paper, we present a method for quantifying climate feedbacks based on "radiative kernels" which describe the differential response of the top-of-atmosphere radiative fluxes to incremental changes in the feedback variables. The use of radiative kernels enables one to decompose the feedback into one factor that depends on the radiative transfer algorithm and the unperturbed climate state, and a second factor that arises from the climate response of the feedback variables. Such decomposition facilitates an understanding of the spatial characteristics of the feedbacks and the causes of intermodel differences. This technique provides a simple and accurate way to compare feedbacks across different models using a consistent methodology. Cloud feedbacks cannot be evaluated directly from a cloud radiative kernel because of strong nonlinearities, but they can be estimated from the change in cloud forcing and the difference between the full-sky and clear-sky kernels. We construct maps to illustrate the regional structure of the feedbacks and compare results obtained using three different model kernels to demonstrate the robustness of the methodology. Our results confirm that models typically generate globally-averaged cloud feedbacks that are substantially positive or near neutral, unlike the change in cloud forcing itself which is as often negative as positive.

1. Introduction

Climate models exhibit a range of sensitivities in response to increased greenhouse gases due to differences in feedback processes which amplify or damp the initial radiative perturbation (Cubasch and Cess, 1990). Analyzing these feedbacks is therefore of central importance to our understanding of climate sensitivity. However, the analysis of feedbacks in GCMs has a potential for ambiguity not present in the analysis of simple steady state models, due to the time dependence and correlations between different feedback variables.

There are two widely-used, but very different, approaches for quantifying climate feedbacks in GCMs. The first method, introduced by Wetherald and Manabe (1988), uses offline calculations to compute the change in radiative fluxes that results from substituting one variable at a time from the perturbed climate state into the control climate. This procedure can be computationally expensive, and there are complexities in its implementation which often lead to spurious differences between feedback calculations performed by different groups (Colman 2003, Soden et al. 2004). The second method uses prescribed sea surface temperature (SST) perturbations to induce a change in top-of-atmosphere (TOA) radiative fluxes (Cess et al., 1990, 1996). The resulting changes in radiative fluxes are then used to infer the climate sensitivity of the model, with the difference between total and clear-sky flux changes providing a measure of the contribution of clouds to this sensitivity. This method of feedback assessment does not isolate the effects of feedback variables other than clouds, such as water vapor and snow/ice albedo. Moreover, a substantial part of the change in cloud forcing does not result from a change in cloud properties, but from cloud masking of the clear-sky response, so that the change in cloud forcing does not accurately reflect the cloud feedback (Zhang et al. 1994, Colman 2003, Soden et

al. 2004).

In this study, we present an alternative method for calculating climate feedbacks which separates the feedback into two factors. The first, termed the "radiative kernel", depends only on the radiative algorithm and the base climate. The second, termed the "climate response pattern", is simply the change in the mean climatology of the feedback variable between two climate states. The product of these two quantities determines the climate feedback for that variable. We show that this technique provides a simple and accurate method for quantifying climate feedbacks. It can also be performed consistently across models; therefore intermodel differences in the estimated feedbacks arise solely from differences in their climate response and not from differences in methodology. The accuracy of this method is assessed by comparing kernel-based estimates of the feedbacks from those derived using a more conventional offline method. We further demonstrate the robustness of this procedure by comparing feedback estimates from three different radiative kernels.

2. Background

Given a direct radiative forcing G, the climate system restores radiative equilibrium at the top of the atmosphere (TOA) by inducing a change in surface temperature T_s and in other aspects of the climate. In this paper, we assume that the radiative forcing is known and does not change in response to the climate state. We also restrict attention to the analysis of models in which the stratosphere has been allowed to adjust to the changes in radiative forcing and tropospheric climate, allowing us to focus on the TOA rather than tropopause fluxes.

Let $R(\mu) = Q(\mu)-F(\mu)$ be the net TOA flux in some climate state, as a function of geographical position, time of year, and time of day, all denoted by the index μ, where F is the outgoing longwave and Q the absorbed shortwave component. For simplicity, consider R as a function of the column distribution of water vapor w, temperature T, a set of clouds properties c and surface albedo a, so that $R = R(w, T, c, a)$. Due to internal variability, particularly synoptic variability, one needs to average over an ensemble of realizations of these state fields, and, therefore, R; in practice, one time averages so as to retain the seasonal and diurnal cycles. We denote this average by an overbar: $\overline{R}(\mu)$.

Suppose that one has two climate states, A and B, where B is a perturbation from A obtained by changing a set of parameters by small amounts. In order to separate the effects of changes in water vapor, for example, from changes in other inputs to the radiative transfer, the standard procedure, introduced by Wetherald and Manabe (1988), is to take water vapor from state B and substitute it into the instantaneous flux computation for A, holding all other inputs (T, c, a) fixed, and then averaging:

$$\delta_w \overline{R} = \overline{R(w_B, T_A, c_A, a_A)} - \overline{R(w_A, T_A, c_A, a_A)} \tag{1}$$

Everything here is a function of μ. Attention is often focused on averages over μ, in particular on the global, annual mean of $\delta_w \overline{R}$. Assuming that the climatic radiative response is linear, the total perturbation arising from a change in climate can be written in terms of the partial radiative perturbations from each feedback variable, $\delta\overline{R} = \delta_w \overline{R} + \delta_T \overline{R} + \delta_c \overline{R} + \delta_a \overline{R} = -G$ which may be further separated into its longwave and shortwave components. A feedback parameter for each variable X can then be written as $\lambda_X = -\frac{\delta_X \overline{R}}{\delta X}\frac{\delta X}{\delta T_s}$ for $X = T, c, w, a$ such that $\delta T_s = - G/\lambda$, where

$\lambda = (\lambda_w + \lambda_T + \lambda_c + \lambda_a)$ which may also be separated into its longwave and shortwave components.

We refer to this approach as the partial radiative perturbation (PRP) method. As pointed out by Colman and McAvaney (1997), a problem with PRP is that it assumes all fields are temporally uncorrelated with each other. Such an assumption can introduce substantial biases in the feedback estimates for fields which are highly correlated. For example, because clouds tend to be optically thick, their presence masks the impact of changes in water vapor at or below the cloud level. Because clouds form during periods of elevated water vapor concentrations, the effect of cloud masking diminishes the impact of the water vapor on the TOA fluxes relative to what would occur under clear sky conditions. By mixing water vapor and cloud profiles from independent simulations, the PRP method eliminates this correlation and biases both the cloud and water vapor feedback calculations.

3. A Conceptual Model of Cross-Field Correlations

To understand this problem it is useful to have a simple thought experiment in mind, constructed in such a way that clouds and water vapor are correlated. Focus on long wave fluxes only and assume that high cloud is present a fraction *f* of the time. When it is present, the flux is always equal to the same constant, which we set to zero for convenience. When it is absent, the outgoing flux is a linear function of water vapor, $\alpha + \beta w$, where β is negative so that the outgoing flux decreases with increasing vapor The water vapor in the cloud free region is w_1, while the vapor underneath the high clouds is w_2.. The average incoming flux is simply

$$\overline{R} = -(1-f)(\alpha + \beta w_1) \tag{2}$$

Now consider a climate change in which the variables f, w_1 and w_2 change by small amounts. The resulting change in R is a sum over cloud and water vapor feedbacks:

$$\delta\overline{R} = \delta_c \overline{R} + \delta_w \overline{R} \tag{3}$$

where

$$\delta_c \overline{R} = (\alpha + \beta w_1)\delta f \tag{4}$$

and

$$\delta_w \overline{R} = -(1-f)\beta\delta w_1 \tag{5}$$

Note that the "cloud radiative forcing", the difference between the actual flux and the clear sky flux, is

$$C_{RF} = f(\alpha + \beta w_2)$$

so that the change in cloud forcing when the climate is perturbed is

$$\delta C_{RF} = (\alpha + \beta w_2)\delta f + f\beta\delta w_2$$

The change in cloud forcing depends only on w_2, whereas the cloud feedback depends only on w_1.

Using PRP in this thought experiment, decorrelation implies that in computing $\overline{R(w_B, c_A)}$, the radiation would see w_{2B} a fraction f_B of the time and w_{1B} a fraction (1 - f_B) of the time, so that

$$\overline{R(w_B, c_A)} = -(1-f_A)[\alpha + \beta(f_B w_{2B} + (1-f_B)w_{1B})] \tag{6}$$

and

$$\delta_w \overline{R} = -\beta(1-f_A)[(w_{1B} - w_{1A}) + f_B(w_{2B} - w_{1B})] \tag{7}$$

or, assuming small perturbations, and not distinguishing between A and B when multiplied by a

perturbation quantity,

$$\delta_w \overline{R} = -\beta(1-f)\delta w_1 - \beta(1-f) f (w_2 - w_1) \tag{8}$$

The last term in this expression corrupts the expected result in Eq. 5. We expect that $w_2 > w_1$ and that the strength of the water vapor feedback is overestimated by PRP. A key deficiency is that this added term is not a perturbation quantity. No matter how small in absolute terms, it will dominate if the perturbation considered is small enough and disrupt any careful attempt to study feedbacks as a function of the size of the perturbation.

The most direct approach to correcting this problem is to compute the effects of decorrelating *w* and *c* directly by using another realization of the unperturbed model *A*. Taking *c* from the second realization (denoted by a prime) and *w* from the first, one obtains, in our thought experiment

$$\overline{R(w_A, c_A^{'})} = -(1-f_A)[\alpha + \beta(f_A w_{2A} + (1-f_A) w_{1A})] \tag{9}$$

Now substituting w_B for w_A and then differencing the two expressions, one is comparing two models in both of which the water and clouds have been decorrelated:

$$\overline{R(w_B, c_A)} - \overline{R(w_A, c_A^{'})} = -\beta(1-f_A)[(w_{1B} - w_{1A}) + f_B(w_{2B} - w_{1B}) - f_A(w_{2A} - w_{1A})] \tag{10}$$

or

$$\overline{R(w_B, c_A)} - \overline{R(w_A, c_A^{'})} = -\beta(1-f)\delta w_1 - \beta(1-f)\delta(f(w_2 - w_1)) \tag{11}$$

In the process we have replaced the unwanted O(1) term with an O(ε) term.

One can obtain a similar result by symmetrizing the standard calculation in A and B, as suggested by Colman and McAvaney (1997) by performing a two-sided PRP. That is, one computes

$$\frac{1}{2}[\overline{R(w_B, c_A)} - \overline{R(w_A, c_A)} + \overline{R(w_B, c_B)} - \overline{R(w_A, c_B)}] \tag{12}$$

In our conceptual model, this eliminates the O(1) term once again, leaving behind a somewhat different O(ε) error. After some manipulation one finds

$$\delta_w \overline{R} = -\beta(1-f)\delta w_1 + \frac{1}{2}[-(1-f)\beta\,\delta(f(w_2 - w_1)) + \beta f(w_2 - w_1)\delta f] \tag{13}$$

4. Radiative Kernels

Rather than replacing w_A by w_B, as in the PRP method, a simple and attractive alternative is to replace w_A with $w_A + \delta\overline{w}$, where $\delta\overline{w}$ is the difference in the mean water vapor between B and A. The resulting vapor input into the radiative flux computation has the same ensemble mean as does w_B but does not perturb correlations. In our thought experiment, the mean vapor is

$$\overline{w} = (1-f)w_1 + fw_2$$

so the change in vapor as the climate is perturbed is

$$\delta\overline{w} = \overline{w_B} - \overline{w_A} = \delta w_1 + \delta(f(w_2 - w_1)) \tag{14}$$

The result is that

$$\overline{R(w_A + \delta\overline{w}, c_A)} - \overline{R(w_A, c_A)} = -\beta(1-f)\delta w_1 - \beta(1-f)\delta(f(w_2 - w_1)) \tag{15}$$

precisely the estimate obtained by explicitly decorrelating.

The technique of perturbing the mean has the advantage of requiring fewer computations of R than does the two-sided PRP method. More importantly, it provides a method of cleanly separating the part of the flux response that is a function of the unperturbed climate from that part that is a function of the perturbation. Since $\delta\overline{w}$ is small, unlike the instantaneous w_B- w_A, and generalizing to include other variables, we can write

$$\overline{R(w_A+\delta\overline{w},T_A,c_A,a_A)}-\overline{R(w_A,T_A,c_A,a_A)}\approx\overline{\frac{\partial R}{\partial w}(w_A,T_A,c_A,a_A)}\,\delta\overline{w}\equiv K^w\delta\overline{w} \tag{16}$$

The factor K describes the differential response of TOA radiation to changes in w. The extraction of K, which depends only on the control climate, explicitly or implicitly underlies most discussions of water vapor feedback.

It is important to break up the flux response to water vapor perturbations into parts due to perturbations in different levels of the troposphere, since different physical mechanisms control the water vapor responses in these different areas. One could analyze the sensitivity to water vapor at different levels using explicit decorrelation, or the two-sided PRP method (Colman and McAvaney 1997), but the method of perturbing the mean provides a simpler framework for estimating these sensitivities.

To simultaneously consider the effects of water vapor at all levels in the vertical we discretize and denote the column of vapor by a vector with elements w_i and write

$$\overline{R(w_A+\delta\overline{w},T_A,c_A,a_A)}-\overline{R(w_A,T_A,c_A,a_A)}\approx\sum_i\overline{\frac{\partial R}{\partial w_i}}\,\delta\overline{w_i}\equiv\sum_i K_i^w\delta\overline{w_i} \tag{17}$$

The vector K_i^w is a function of μ = (geographical position, time of year, time of day). We refer to $K_i^w(\mu)$ as the water vapor response kernel. It provides the information needed to analyze a model's water vapor feedback in a succinct form. To the extent that K is insensitive to the model used to compute it, one can compare water vapor feedbacks in different models simply by multiplying $K_i^w(\mu)$ by the different vapor responses $\delta w_i(\mu)$.

Rather than use an additive constant to change the mean value of the vapor, one can use a multiplicative constant. This is equivalent to thinking of the logarithm of the water vapor as one's input into *R*. Although it makes no difference for infinitesimal perturbations, linearity is a better approximation for perturbations of the size typically encountered in climate change studies if one uses *ln*(*w*) as the variable, since absorption of radiation by water vapor is roughly proportional to ln(w).

One can compute the response to temperature perturbations in an exactly analogous fashion to water vapor:

$$\overline{R(w_A, T_A + \delta\overline{T}, c_A, a_A)} - \overline{R(w_A, T_A, c_A, a_A)} \approx \sum_i \overline{\frac{\partial R}{\partial T_i}} \delta\overline{T_i} \equiv \sum_i K_i^T \delta\overline{T_i} \tag{18}$$

And for surface albedo:

$$\overline{R(w_A, T_A, c_A, a_A + \delta\overline{a})} - \overline{R(w_A, T_A, c_A, a_A)} \approx \frac{\partial R}{\partial a} \delta\overline{a} \equiv K^a \delta\overline{a} \tag{19}$$

In our thought experiment, all of the methods described that avoid the major part of the contamination resulting from decorrelating *w, T, c,* and *a* still retain errors proportional to the size of the perturbation. In our conceptual model, one can obtain the exact result immediately if one knows from the start that the only variables that *R* depends on are the vapor w_1 in cloud-free areas and the cloud fraction *f*. The question of how to proceed in general to find appropriate variables so as to minimize biases is an interesting one that we do not pursue here.

5. Results

To estimate these response kernels, we use a control integration of the GFDL AM2 atmospheric

model (version AM2p12b) as described in GAMDT et al. (2004). The only difference from the model described in that paper is that we use climatological, seasonally-varying sea surface temperatures and sea ice distributions. A radiative flux computation is performed 8 times daily during a 1 year simulation, while simultaneously archiving the full input into every radiative calculation. We then rerun the full radiative computation off-line 2N+2 times, where N is the number of model layers (24), perturbing, in turn, the temperature and specific humidity in each layer, followed by surface temperature and albedo. Experimentation indicates that one year is adequate for estimating the zonal and annually averaged kernels, but that multi-year simulations would be needed to obtain accurate local maps of feedback strengths in some regions.

Instantaneous temperatures, including the surface skin temperature, are perturbed by 1K. Instantaneous humidities are perturbed by a multiplicative factor that results from the increase in saturation specific humidity corresponding to a 1 K warming, while holding the relative humidity constant. As temperatures increase by $\delta\overline{T}$, mixing ratios must increase by $\xi\delta\overline{T}$ where

$$\xi \equiv \frac{\overline{w_i}}{\overline{w_i^s}} \frac{dw_i^s}{dT} \tag{20}$$

if they are to maintain a fixed mean relative humidity. Here $\overline{w_i^s}$ is the saturation specific humidity at the monthly-mean temperature and pressure for this point. To make it easier to compare K^T with K^w, and to assist in the analysis of models in which changes in tropospheric relative humidity are small, we define $K_i^\omega = K_i^w \xi$ and $\delta\omega_i = \delta w_i / \xi$, so that

$$K_i^\omega \delta\omega_i = K_i^w \delta w_i \tag{21}$$

We make all these computations for clear skies (i.e. clouds instantaneously set to zero) as well as for the total sky conditions simulated by the model. After perturbing each model layer in this

way, we then mass-average the resulting kernels, using the monthly-mean pressure distribution, to compute the response to perturbations in 100mb thick layers.

We are interested in the sensitivity of the TOA flux to tropospheric perturbations. When we present tropospherically-averaged results below, we integrate from the surface up to the tropopause, defined as 100mb at the equator and increasing linearly with latitude to 300mb at the poles. In our experience, it is simpler and more accurate to consider TOA fluxes, rather than tropopause-level fluxes, the latter being more sensitive to the precise definition of the tropopause due to the vertical gradient in flux near the tropopause. If not carefully accounted for, a change in height of the tropopause due to a climate perturbation will itself result in a non-negligible change in "tropopause level" fluxes. In contrast, the vertical integration of the contributions to the TOA fluxes from the troposphere is less sensitive to this definition, as the contribution from layers near the tropopause is generally small. The results presented here are not sensitive to our choice of a simple pressure-based tropopause definition versus a lapse-rate definition.

5. 1 Temperature Kernel

The temperature kernel, K^T, describes the response of the longwave TOA fluxes to incremental increases in temperature of 1K and has units of W/m^2/K/100mb. The result is averaged over the year and over longitude to generate the latitude-pressure plot shown in Fig. 1 (top). To the extent that K^T has seasonal, diurnal or longitudinal structure, this average would not be sufficient for computing the TOA flux response to a temperature perturbation with significant seasonal, diurnal, or longitudinal variations. The clear sky analogue of this plot is presented in Fig. 1 (middle). Due to its much larger emissivity, the surface contribution is an order of magnitude

larger than that from any individual 100mb atmospheric layer and for display purposes is depicted as a separate figure (bottom).

If temperatures change uniformly, Fig. 1 illustrates the contribution of different latitudes and levels to the change in TOA longwave fluxes. The values are negative, indicating that an increase in temperature decreases the net incoming radiation (i.e., increases the OLR). Under clear-skies, the sensitivity of longwave fluxes to temperature changes is largest in the tropics owing to the greater sensitivity of the Planck emission at higher temperatures. Low sensitivities occur near the tropopause at all latitudes and near the surface at high latitudes reflecting regional differences in lapse rate and emissivity. The function K^T is also strongly affected by clouds. Under total-sky conditions the longwave fluxes are most sensitive to temperatures at the level of cloud tops that are exposed to space. This results in an obvious maximum just beneath the tropopause, where convectively detrained cirrus anvils are common, and along the top of the cloud-topped boundary layer. By masking the surface, clouds also diminish the surface contribution to K^T. The vertically-integrated global, annual mean of K^T for clear and total sky conditions is -3.6 W/m^2/K and -3.3 W/m^2/K respectively, indicating that by lowering the mean emission temperature, clouds also reduce the longwave flux sensitivity.

5.2 Water Vapor Kernel

Proceeding in the same way for the water vapor response, we show the results for K^ω for both total and clear skies in Fig. 2. Assuming that temperatures change uniformly and that the relative humidity remains constant, the function K^ω provides insight into the relative importance of different latitudes and levels to the strength of the longwave water vapor feedback. The values

are predominantly positive, as the increase in water vapor acts to increase the net incoming longwave at the TOA. In regions characterized by temperature inversions, such as near the surface at high latitudes, it is possible for an increase in water vapor to decrease, rather than increase, the net longwave flux. Under clear skies, one sees that the deep tropics dominate K^{ω}, with rapidly diminishing contributions as one proceeds towards higher latitudes. The equatorial maximum arises, in part, from the enhanced absorption provided by self-broadening of the water vapor lines under moist, tropical conditions.

Under clear skies, the vertical distribution of K^{ω} is relatively uniform within the tropical free troposphere, indicating that all levels would be of comparable importance to water vapor feedback if temperature changes are uniform and if relative humidity remains unaltered. However, clouds strongly modify the distribution of K^{ω} by preferentially masking the effects of lower level moistening. The result is to reduce the overall magnitude of K^{ω} while also shifting peak values to the tropical upper troposphere, and in particular to the dry regions of the subtropical belts where upper level clouds are scarce. The vertically-integrated global, annual means of K^{ω} for clear and total sky conditions are 1.62 W/m^2/K and 1.13 W/m^2/K respectively (Table 1). By masking underlying water vapor perturbations, clouds reduce the sensitivity of OLR to water vapor changes and increase the relative importance of upper tropospheric moistening to the total feedback.

Water vapor also absorbs solar radiation, and the enhanced absorption under moister climates provides a smaller, but non-trivial, contribution to the total feedback from water vapor. The shortwave kernels for water vapor absorption corresponding to a uniform warming and constant

relative humidity moistening are shown in Fig. 3. The values are again positive, indicating that the increased water vapor acts to increase the net incoming solar radiation (i.e., it results in increased solar absorption). The magnitudes are roughly a factor of 5-10 smaller than those computed for the longwave part of the spectrum, except at high latitudes. Due to the weaker line strengths in the solar part of the spectrum, the shortwave sensitivity is largest in the lower levels where the vapor concentrations are largest. Maxima occur over the highly reflective snow and ice surfaces near the poles, which increase the probability of absorption by reflecting photons back up through the atmosphere. Similarly, clouds act to increase the strength of water vapor feedback in the solar spectrum by increasing atmospheric radiation path lengths through reflections. The vertically-integrated global, annual mean of the shortwave K^{ω} for clear and total sky conditions is 0.16 W/m^2/K and 0.27 W/m^2/K respectively (Table 1). The presence of clouds serves to increase the height of peak sensitivity relative to clear sky conditions while also diminishing the absorption at lower levels.

If temperature changes are uniform and relative humidities remain unchanged as the climate warms, the shortwave and longwave kernels can be summed to compute the total radiative sensitivity to water vapor perturbations. Under this idealized scenario, the shortwave plus longwave feedback is 1.78 W/m^2/K for clear sky and 1.40 W/m^2/K for total sky conditions. The humidity response in the free troposphere (above 800 hPa) is responsible for ~90% of the water vapor feedback, of which roughly two-thirds originates in the tropics (30*N*–30*S*). The majority of this tropical free-tropospheric contribution (~40% of the total feedback) arises from the upper half of the tropical free troposphere (100–500 hPa).

5.3 Model Simulated Response Patterns

The temperature and humidity changes predicted by climate models are not spatially uniform. Climate models predict that warming in the tropics will be larger in the upper troposphere than in the lower troposphere and that there will be some local changes in relative humidity. To compute the feedback corresponding to a particular climate model projection, one simply multiplies the appropriate kernels by the model-predicted temperature $d\overline{T}_i$ and water vapor $d\overline{\omega}_i$ responses. As an example, we use the zonal-annual mean of $d\overline{T}_i$ and $d\overline{\omega}_i$ from an idealized climate change experiment with the GFDL AM2p12b GCM, in which the climatological SSTs are perturbed by +/- 2K in all seasons (see Soden et al. 2004 for details of these experiments). Multiplying the 4-dimensional response patterns by the corresponding 4-dimensional total-sky kernels K^T and K^ω in Fig. 1-3 for each month, latitude, longitude, and level, and then averaging over longitude and time, yields the height-latitude structure of total-sky TOA flux responses shown in Fig. 4 for temperature (top) and water vapor (middle). Compared to the uniform warming response (Fig 1), the model-predicted flux response portrays greater sensitivity to the tropical upper troposphere, owing to the reduction in tropical lapse-rate and resulting increase in Planck emission per unit warming of the surface. However, because this model closely follows a constant relative humidity moistening, the increased Planck emission is largely offset by the increased water vapor opacity (Fig. 4, middle). As shown below, this is a common feature of all current GCMs.

Fig. 4 (bottom) shows the contributions to the water vapor feedback that result from departures from constant relative humidity in the model. The results are computed by multiplying the shortwave and longwave water vapor kernel by the difference of $d\overline{T}_i - d\overline{\omega}_i$. The units are also in

$W/m^2/K/100$ hPa. Positive values indicate regions where the relative humidity has increased as the surface warmed, resulting in an increase in the net upward radiation at the TOA relative to its constant relative humidity value. The model's relative humidity does change in response to a surface warming and, locally, these changes can be large relative to the total water vapor feedback. For this particularly idealized scenario, the uniform surface warming has resulted in an increase in relative humidity in the equatorial free troposphere which is offset by decreases in relative humidity in the subtropical free troposphere. Other regions of increased relative humidity occur near the top of the troposphere due to the upward shift of the tropopause as the climate warms. Locally the mid-tropospheric changes can be as large as 25% of the overall water vapor feedback. However, when vertically integrated and globally averaged, the feedback is within 5% of that expected from a constant relative humidity change in water vapor.

5.4 Surface Albedo Feedback

We also compute a surface albedo kernel K^{α} which describes the response of downward shortwave radiation at the TOA to a 1% additive increase in surface albedo. In contrast to the 4-dimensional temperature and water vapor kernels, after diurnally averaging the K^{α} is only a function of latitude, longitude and month of year. Values of the total-sky K^{α} are greatest in low latitudes where the incident solar radiation is largest. Because clouds act to mask the effects of any underlying change in surface albedo, K^{α} tends to be smallest in regions of persistent cloud cover, such as the mid-latitude storm tracks, and largest in regions which are relatively free of clouds, such as low-latitude deserts. The methodology is applicable to any cause of surface albedo change, however there is potential for nonlinearity in the interaction between clouds and surface albedo, to the extent that large cloud responses follow the boundaries of the snow or ice

cover. Shell et al. (2007) find that clear-sky shortwave flux changes in the mixed-layer version of NCAR's Community Atmospheric Model (which includes variations in sea ice) are underestimated by about a quarter in a doubled CO2 experiment. The underestimation is significantly reduced when 3-hourly values are used, as here, rather than monthly averages.

5.5 Comparison to the PRP Method

Table 2 compares the climate feedbacks for temperature, water vapor and surface albedo estimated using the kernels with that obtained via the standard PRP method. Following Colman and McAvaney (1997), and as described above, two sets of substitutions are performed to remove the effects of field decorrelation. The results from inserting perturbed fields from the +2 K simulation with control fields from the -2 K simulation is referred to as the "forward PRP" in Table 2, and the opposite is referred to as "reverse PRP". The last column lists the average of the two substitutions following eq. (12) and contains the results to which the kernel feedbacks should be compared.

For simplicity, the change in TOA fluxes from the PRP method is compared to the kernel flux perturbations that have been integrated from the surface to the TOA. This eliminates the difficulties that arise from attempting to define flux changes at the tropopause in simulations for which the tropopause height changes in response to a climate perturbation.

For the forward perturbation, the water vapor feedback is ~6% larger than that estimated from the kernels. Because clouds tend to be associated with higher concentrations of water vapor, the forward decorrelation acts to exaggerate the impact of the change in water vapor. The reverse is

true for the backward substitution, resulting in a ~10% underestimate of the water vapor feedback. However, the average of the forward and backward PRP substitutions acts to remove the first order effects of this decorrelation and agrees to within ~3% with the kernel estimate. Similar effects of decorrelation are seen for the temperature and surface albedo feedbacks. In all cases, the kernel-estimated feedback agrees to within 3% of the average of the forward and reverse PRP calculation. From the analysis of the thought experiment outlined above, the one-sided PRP calculations can be expected to become more inaccurate for smaller perturbations.

A limitation of the kernels is that the radiative effects of clouds, particularly the vertical overlap of clouds, are too non-linear to accurately compute cloud feedback using this method. If one knows the total change in TOA fluxes as simulated by the model (and the magnitude of any imposed TOA radiative forcing) one can compute the cloud feedback as a residual (e.g., Soden and Held 2006). The results of this residual estimate of cloud feedback (listed in Table 2 under the kernel column) agree to within ~10% with the explicitly-computed cloud feedback using the PRP method. Since there is no radiative forcing imposed in this +2/-2 K SST climate change experiment, this does not represent an additional source of error in the residual cloud feedback estimate. However, in simulations for which a radiative forcing is imposed, the uncertainties in radiative forcing may be comparable to or larger than the errors noted here. An alternative approach to estimating cloud feedbacks using these kernels is outlined in Sec. 5.8 below.

5.6 Intercomparison of Kernels from Different Models

To the extent that the kernels themselves do not vary significantly between models, one can use pre-computed kernels to easily convert the climatic changes in feedback variables into feedback

strengths. In addition to being computationally simple, this also facilitates the comparison of feedbacks among different models.

To investigate the robustness of the kernels, plots on the left side of Fig. 5 compare the zonal-mean, annual-mean distribution of K^T computed from the GFDL (top), NCAR (middle) and BMRC (bottom) climate models for total-sky conditions. The corresponding water vapor kernels K^ω are shown on the right side of Figure 5. The models all show the same basic height-latitude structure, with maxima in K^T following the distribution of cloud tops and maxima in K^ω located in the tropical upper troposphere. Local differences in the kernels typically range from 10-20%. The intermodel differences arise from both differences in the radiative transfer algorithms and differences in the base climatology between models. Given their strong impact on the TOA radiation, differences in the climatological distribution of clouds between the models are a key contributor to discrepancies in the kernels. For example, the GFDL model tends to have greater amounts of high cloud cover in the tropics which results in larger values of K^T in these regions due to the increased emissivity from the cloud tops, and smaller values of K^T from underlying layers due to the increased masking effects. Similar impacts of cloud cover differences between models are apparent in K^ω.

When vertically integrated, the zonal-mean kernels agree to within ~10% (Figure 6) with the notable exception of the high-latitude southern hemisphere where differences reach ~30%. When globally-averaged, the range in K^T and K^ω among the three models examined here are roughly 5% or less (Table 3). For reference, the global-mean, vertically integrated kernels for clear skies are also listed in Table 3 (in parentheses). Interestingly, the differences among clear-sky kernels

are comparable in magnitude to the total-sky differences, suggesting that clouds are not the primary cause of discrepancy for the global-mean kernels. Note that the results for K^{α} in Table 3 are expressed in units W/m^2 per 1% decrease in surface albedo.

To further investigate the extent to which differences in radiative transfer algorithms can contribute to the intermodel differences, a second set of kernels was computed for the BMRC model using the same base climatology but with a newer radiative transfer algorithm based on the Sun-Edwards-Slingo (SES) parameterization (Sun and Rikus, 1999) instead of the older algorithm which is based on the Fel and Schwarzkopf (1975) and Lacis and Hansen (1974) parameterizations. These SES results are also listed in Table 3. Information on the GFDL and NCAR radiation codes can be found in GAMDT (2004) and Collins et al. (2006) respectively. The global-mean temperature kernels are very similar, however the water vapor kernel is ~10% larger (more negative) for the SES kernel compared to the LH/FS kernel. Thus, it is possible that some of the difference between the GFDL, NCAR and BMRC kernels stems from differences in the parameterization of radiative transfer. However, it should be noted that the LH/FS code is based on a much older algorithm than those currently in use in these three models.

In principle, one would prefer to compute kernels using a line-by-line (LBL) radiative transfer code to avoid uncertainties in the parameterization of the narrow-band transmission. But such calculations are computationally expensive. While there are many comparisons of fluxes between LBL and band models, there is relatively little discussion in the literature concerning the differences in the response of these fluxes to perturbations in temperature or water vapor. Recently, Huang et al. (2006) have compared the differential responses of OLR to temperature

and water vapor perturbations from the GFDL narrow-band radiation code used here with those obtained from line-by-line calculations for a limited number of profiles; the analysis was restricted to clear-sky fluxes. When vertically-integrated, Huang et al. found differences between the flux responses in the LBL and narrow-band GFDL radiation code of less than 1% for water vapor perturbations and less than 5% for temperature perturbations.

5.7 Feedbacks from the IPCC AR4 Model Simulations

Recently, Soden and Held (2006) estimated the range of feedback strengths in current models using the GFDL radiative kernels and an archive of 21st century climate change experiments performed for the IPCC AR4. In this sub-section, we repeat their analysis using radiative kernels from the NCAR and BMRC models to examine the sensitivity of the feedback estimates to different model representations of the kernels. Following Soden and Held (2006), feedback calculations are performed for climate change simulations from 14 different coupled ocean-atmosphere models integrated with projected increases in well-mixed greenhouse gases and aerosols as prescribed by the IPCC SRES A1B scenario. This scenario corresponds roughly to a doubling in equivalent CO_2 between 2000 and 2100, after which time the radiative forcings are held constant. Unfortunately, information on the radiative forcing for different models and different scenarios is not available from the IPCC AR4 archive. Therefore we use the IPCC TAR values of radiative forcing under this scenario (4.3 W/m^2) which has an estimated uncertainty of 10% (Table 6.14 and 6.15). We note, however, this may underestimate the true intermodel range in radiative forcing, particularly when aerosols are involved. For example, a recent study by Collins et al. (2007) noted that the intermodel range of longwave forcings at the top-of-atmosphere forcings from well-mixed greenhouse gases for the period 1860 to 2000 was 1.5 to

2.7 Wm^{-2}. Because uncertainty in radiative forcings used in the IPCC AR4 models directly impacts our residual-based estimates of cloud feedback, we also describe an alternative approach for estimating cloud feedback (section 5.8) which is considerably less sensitive to the assumed value and spatial distribution of radiative forcing.

As in Sec. 2, we set $\Delta\overline{T_s} = \frac{\Delta\overline{R}}{\overline{\lambda}}$, where $\lambda = \lambda_T + \lambda_C + \lambda_w + \lambda_\alpha$ and the overbar indicates global averaging. The temperature feedback is further separated into two components: $\lambda_T = \lambda_0 + \lambda_L$, where λ_0 (Planck feedback) assumes that the temperature change is vertically-uniform throughout the troposphere and λ_L (lapse rate feedback) is the departure of the temperature change from that at the surface. For each variable *x*, we compute the feedbacks as product of the radiative kernel and the climatic response: $\lambda_X = K^x dx$. The kernels are computed as described above. The model response *dx* for each variable *x* is computed by differencing the projected climate of years (2000-2010) from that of (2100-2110) and normalizing by the change in global mean surface air temperature. Both K_x and *dx* are functions of latitude, longitude, altitude and month. We do not consider here the possibility of rectification due to correlations between the diurnal cycles of K_x and *dx*. Each λ_x is then vertically-integrated from the surface to the tropopause (defined once again as 100mb at the equator and increasing linearly with latitude to 300mb at the poles) and globally-averaged to yield global feedback parameters.

Figure 7 shows our estimates of the global-mean feedbacks for lapse-rate, water vapor, cloud, and surface albedo for each of the IPCC AR4 models (listed in Table 1 of Soden and Held 2006) and for each of the three model-derived radiative kernels. Cloud feedbacks are computed as a

residual; since we do not have sufficient information on the spatial structure of the radiative forcing from the models, we simply assume that the 4.3W/m^2 estimated radiative forcing for the A1B integrations over the 21st century is distributed uniformly in space and season. The sign convention is such that positive values indicate an amplification of the climate change (i.e., a positive feedback). The strength of λ_0 (not shown) ranges from roughly -3.1 to -3.2 W/m^2/K. This small uncertainty arises from different spatial patterns of warming; models with greater high latitude warming, where the temperature is colder, have smaller values of λ_0. On average, the strongest positive feedback is due to water vapor (~1.9 W/m^2/K), followed by clouds (~0.7 W/m^2/K), and surface albedo (~0.3 W/m^2/K). The troposphere warms faster than the surface in all models resulting in a negative lapse-rate feedback (roughly -1 W/m^2/K).

Overall, the feedback calculations are relatively insensitive to the choice of a particular model's kernel, indicating that uncertainties in the radiative algorithms and in the distribution of radiatively active constituents in the base climate are small compared to the intermodel differences in climate response. The largest sensitivity is for the surface albedo, where the range from the BMRC kernel is ~30% larger than that derived using the NCAR kernel. The larger sensitivity may reflect a smaller cloud masking of surface albedo changes in the BMRC kernel compared to the GFDL and NCAR kernels. This is consistent with the better agreement between the BMRC and GFDL/NCAR albedo kernels under clear-sky conditions relative to total-sky conditions (Table 3)

Since these estimates of cloud feedback are computed as a residual they contain two potential sources of error: (1) the accumulation of errors in the estimation of other feedbacks; and (2)

uncertainties in the estimate of the effective climate sensitivity which, in turn, depends upon errors in the estimated radiative forcing. For example, the larger values of surface albedo feedback derived using the BMRC kernel result in systematically smaller values of cloud feedback for that kernel in comparison to that estimated from the GFDL and NCAR kernels. This uncertainty is enough to change the sign of cloud feedback in two of the models from weakly positive to weakly negative. However, the conclusion that cloud feedback in current models range from neutral to strongly positive does not appear to be sensitive to the choice of the radiative kernel. Uncertainties in the global-mean radiative forcing used in the models are ~10% (although regional differences are larger) and also unlikely to change this basic conclusion.

Maps of the multi-model ensemble mean feedbacks computed from the GFDL kernel are displayed in Figure 8. Again, the sign convention is such that positive values indicate a positive feedback. The individual feedbacks for each model are expressed in terms of the TOA radiative flux response per degree global warming ($W/m^2/K$) before creating the multi-model ensemble mean. Maxima in the temperature and water vapor feedbacks occur in the tropics where the kernels exhibit their greatest sensitivity and where the largest upper tropospheric temperature and water vapor responses occur. The similarity between the temperature and water vapor feedbacks reflects the close coupling between these variables even at the regional scale. Surface albedo feedbacks are naturally largest over snow and ice covered regions. The corresponding feedback maps for temperature, water vapor and surface albedo under cloud-free conditions are shown in Figure 9. As expected, the most prominent cloud masking of temperature and water vapor feedback occurs over tropical convective regions where high clouds are most frequent.

A rough estimate of the ensemble-mean cloud feedback (Fig. 8) is obtained by residual, assuming that the spatial response of the forcing is uniform. However, the forcing due to greenhouse gases is known to be non-uniform (Ramaswamy et al., 2007) and the existence of aerosol forcing in these A1B simulations makes this assumption particularly problematic. For example, the maxima over southeast Asia, the southeast US and portions of Europe are likely artifacts of this assumption, motivating an alternative approach to estimating cloud feedbacks, to which we now turn.

5.8 *Estimating Cloud Feedback from Changes in Cloud Radiative Forcing*

Here we discuss an alternative method for computing cloud feedback by adjusting the model-simulated change in cloud radiative forcing to account for cloud masking effects. This method avoids the need to compute cloud feedback as a residual term and is less sensitive to uncertainties in the external radiative forcing imposed on the models.

Cloud radiative forcing is defined as the difference in the TOA fluxes between cloud free and all-sky conditions

$$C_{RF} \equiv R(T,\, w,\, c,\, a) - R(T,w,0,a) \tag{21}$$

One can decompose the change in TOA flux (dR) into a change in cloud radiative forcing plus changes in clear sky fluxes,

$$dR = dC_{RF} + K_T^0 dT + K_W^0 dW + K_a^0 da + G^0 \tag{22}$$

where the K^0's are the clear-sky kernels and G^0 is the clear sky forcing. Or one can decompose R into a sum of the total-sky flux responses,

$$dR = \delta_c R + K_T dT + K_W dW + K_a da + G \tag{23}$$

where ($\delta_c R$) is the cloud feedback, *K*'s are the total-sky kernels, and *G* is the total-sky forcing. Equating (22) and (23) we can relate a change in cloud radiative forcing to a cloud feedback,

$$\delta_c R = dC_{RF} + (K^0{}_T - K_T)dT + (K^0{}_W - K_W)dW + (K^0{}_a - K_a)da + (G^0 - G) \qquad (24)$$

The clear and full sky kernels needed to convert cloud forcing to cloud feedback have been described above. For model experiments in which there are forcing changes, the term G^0-G must also be included. For a 2XCO2 perturbation, using the GFDL radiation code and control climate, we estimate that cloud masking reduces the global average radiative forcing by $(G^0\text{-}G)/G$ ~0.16. For simplicity we assume the same proportionality of cloud masking occurs under the A1b scenario for which G ~4.3 W/m^2, resulting in $(G^0\text{-}G)$ ~0.69 W/m^2. When estimating the spatial structure of the cloud feedback, we simply assume that the difference between clear and full sky forcing is spatially uniform. Because this difference is much smaller than G itself, this limitation is of much less concern than when attempting to compute cloud feedback as a residual form the full sky computation alone.

Differencing the clear-sky and full-sky feedback maps from the IPCC AR4 models (Fig. 8-9) yields a multi-model estimate of the adjustments to dC_{RF} (Fig 10) for the temperature (upper left), water vapor (upper right) and surface albedo (lower left) terms based upon the GFDL kernel. The sum of all three components (lower right) plus the estimated masking effects from the radiative forcing component represents the total offset which should be added to a change in cloud radiative forcing to yield the corresponding estimate of cloud feedback.

Figure 11 compares the multi-model ensemble-mean cloud feedback from Soden and Held (2006) which was estimated as a residual using the total sky kernel method (top) with the

uncorrected change in cloud radiative forcing (middle). The results are restricted to the 11 models in the AR4 archive for which output necessary to calculate cloud feedbacks and cloud radiative forcing is available. There are similarities in the spatial patterns of these two fields, although the change in cloud forcing is clearly much smaller in magnitude than this residual estimate of cloud feedback. Moreover, the ensemble-mean dC_{RF} is substantially negative (-0.22 W/m^2/K) for these models, whereas the estimated cloud feedback for the same subset of models is strongly positive (0.77 W/m^2/K). The lower panel in Figure 11 shows the change in cloud forcing after the cloud-masking adjustments have been added, and using for a spatially uniform value of $(G^0\text{-}G)$ ~0.69 W/m^2. The global-mean values are now in much better agreement and the similarity in spatial structure is more evident. Indeed, the two estimates of cloud feedback are in remarkably good quantitative agreement over most of the globe. The corrected CRF response resembles the direct residual approach except over East Asia and Eastern North America and the downwind oceanic regions, where aerosol forcing is largest, suggesting that the corrected CRF response is able to remove much of this aerosol imprint, as desired. This improved estimate of the ensemble mean cloud feedback is positive over all regions except for the high-latitude southern oceans and portions of the north Atlantic and Arctic oceans. Maxima in cloud feedback tend to occur over the eastern side of the ocean basins where low clouds dominate and along the ITCZ. Prominent land maxima are found in over the Amazon and the southern half of Africa.

The global mean dC_{RF} and $\delta_c R$ for each of the 11 models are also presented in Figure 7. After adjusting the dC_{RF} for the effects of cloud masking, both the mean and intermodel distribution of the global means are in very good agreement. Also note that the adjustments to the cloud radiative forcing are not sensitive to the kernel used to compute them. The global mean offsets

are 0.66 W/m^2/K (GFDL), 0.68 W/m^2/K (NCAR), and 0.48 W/m^2/K (BMRC) and their spatial distributions are nearly identical as that shown for the GFDL model (Figure 10) reflecting the similarity in the climatological distribution of cloud cover .

6. Summary

In this paper, we use radiative kernels as a tool for analyzing radiative climate feedbacks in models. Radiative kernels describe the differential response of the top-of-atmosphere radiative fluxes to incremental changes in the feedback variables. They enable a climate feedback to be decomposed into two factors - one that depends on the radiative transfer algorithm and the unperturbed climate state and a second that arises from the climate response of the feedback variables. This factorization isolates the components of the feedback which are intrinsic to the radiative physics from those which arise from a particular pattern of climate response. This also quantifies GCM feedbacks in a manner that is consistent with the simple analysis common in steady state models.

We demonstrate several benefits to using radiative kernels. The separation of the radiative and climate response components of the feedbacks enables a better understanding of the underlying physical processes which give rise to the feedbacks. This is readily apparent for water vapor and temperature feedbacks, whose vertical response patterns are tightly coupled. Once the kernels are computed, the calculation of model feedbacks is significantly easier to implement than current "partial radiative perturbation" methods and avoids biases which may arise from cross-field correlations. Because a single set of kernels can be used for different climate responses, the

technique also provides an effective way of comparing feedbacks across models (as shown here for the IPCC AR4 simulations) or between different climate change scenarios.

A key limitation of the kernel method is that kernels for cloud feedbacks cannot be computed directly and the PRP method remains an effective tool for further dissecting many aspects of cloud feedback. However, the kernels can be used to estimate the impacts of cloud masking on non-cloud feedbacks (i.e., temperature, water vapor and surface albedo) which have often led to confusion when interpreting changes in cloud radiative forcing (Zhang et al. 1996, Colman 2003, Soden et al. 2004). By differencing the clear-sky and total-sky kernels, we show how changes in cloud radiative forcing can be adjusted to account for these effects. The method of adjusting the cloud radiative forcing is shown to provide a more robust method for describing the regional structure in cloud feedback than either the cloud radiative forcing or residual method. Our results support the picture that global mean cloud feedbacks in the current generation of climate models are generally positive, or near neutral, unlike the changes in cloud forcing, which are often negative.

Acknowledgements: We thank two anonymous reviewers for their comments. We also acknowledge the modeling groups, the Program for Climate Model Diagnosis and Intercomparison (PCMDI) and the WCRP's Working Group on Coupled Modelling (WGCM) for their roles in making available the WCRP CMIP3 multi-model dataset. Support of this dataset is provided by the Office of Science, U.S. Department of Energy.

7. References

Cess, RD and co-authors, 1990: Intercomparison and interpretation of climate feedback processes in 19 atmospheric GCMs, *J. Geophys. Res*., **95**, 16601-16615.

Cess, RD and co-authors, 1996: Cloud feedback in atmospheric general circulation models: An update, *J. Geophys. Res*., **101**, 12791-12794.

Colman, R, 2003: A comparison of climate feedbacks in GCMs, *Clim. Dyn*. **20**, 865-873.

Colman, R and BJ McAvaney, 1997: A study of general circulation model climate feedbacks determined from perturbed SST experiments, *J. Geophys. Res*., **102**, 19383-19402.

Collins, W.D. et al., 2006 : The formulation and Atmospheric Simulation of the Community Atmosphere Model Version 3 (CAM3), *J. Climate*, **19**, 2144-2161.

Cubasch, U and RD Cess, Processes and modeling, in Climate Change: The IPCC Scientific Assessment, 1990, Cambridge Univ. Press, 365 pp.

Fels, S B. and M. D. Schwarzkopf, 1975: The simplified exchange approximation: A new method for radiative transfer calculations. *J. Atmos. Sci*., **32**, 1475-1488.

GAMDT - The GFDL Global Atmospheric Model Development Team, 2004: The new GFDL global atmosphere and land model AM2-LM2: Evaluation with prescribed SST simulations. *J. Climate*, **17**, 4641-4673.

Held, IM and BJ Soden, 2000: Water vapor feedback and global warming, *Ann. Rev. Energy Environ*., **25**, 441-475.

Huang, Y., V. Ramaswamy, and B. J. Soden, 2006: An Investigation of the Sensitivity of the Clear-sky Outgoing Longwave Radiation to Atmospheric Temperature and Water Vapor, *J. Geophys. Res*., in press.

Lacis, A. A. and J. E. Hansen, 1974: A parameterization for the absorption of solar radiation in the earth's atmosphere. *J. Atmos. Sci*., **31**, 118-133.

Shell, K.M., J.T. Kiehl, and C.A. Shields, 2007: Clear-sky radiative feedbacks in NCAR's Community Atmospheric Model. *J. Climate*, in press.

Shine K.P. and A. Sinha 1991: Sensitivity of the earth's climate to height-dependent changes in the water vapour mixing ratio, *Nature*, **354**, 38–84.

Soden, B.J, A. J. Broccoli, and R.S. Hemler, 2004: On the use of cloud forcing to estimate cloud feedback, *J. Climate*, **17**, 3661-3665.

Soden, B.J., and I.M. Held, 2006: An assessment of climate feedbacks in coupled ocean-atmosphere models, *J. Climate*, **19**, 3354-3360.

Spencer, R.W. and W.D. Braswell, 1997: How dry is the tropical free troposphere? Implications for global warming theory. *Bull. Am. Meteorol Soc*., **78**, 1097–106.

Sun, Z. and Rikus, L. 1999: Improved application of ESFT to inhomogeneous atmosphere, J. *Geophys. Res*., **104**, 6291–6303.

Wetherald, RT and S Manabe, 1988: Cloud feedback processes in a general circulation model, *J. Atmos. Sci.,* **45**, 1397-1415.

Zhang, MH, RD Cess, JJ Hack, and JT Kiehl, 1994: Diagnostic study of climate feedback processes in atmospheric GCMs, *J. Geophys. Res*., **99**, 5525-5537.

Figure Captions

Figure 1 The zonal-mean, annual-mean temperature kernel K^T under total sky (top) and clear sky (middle) conditions in units of W/m^2/K/100hPa. The surface component of the kernel is shown separately (bottom) for both total-sky (solid) and clear-sky (dashed).

Figure 2 The zonal-mean, annual-mean water vapor kernel K^ω under total sky (top) and clear sky (bottom) conditions in units of W/m^2/K/100hPa. When multiplied by the vapor response (1 unit of vapor is required to maintain constant relative humidity for a 1K temperature increase), a pressure average of K^ω yields the total effect of the column temperature perturbation on the TOA longwave flux.

Figure 3 Same as figure 2, but for the net downward shortwave radiation at the TOA.

Figure 4 The total-sky TOA flux response due to the temperature perturbations (top) and water vapor (middle) displayed in Fig. 5. The bottom plot shows the portion of the water vapor effect that is due to departures from constant relative humidity. Positive values indicate an increase in net outgoing radiation (i.e., a cooling effect). The results are normalized by the change in global mean surface temperature and are expressed in units of W/m^2/K/100hPa.

Figure 5: The annual-mean, zonal-mean temperature K^T and water vapor K^ω kernels under total sky conditions for the GFDL (top), BMRC (middle) and NCAR (bottom) models in units of W/m^2/K/100hPa.

Figure 6: Zonal, annual-mean of the vertically-integrated temperature K^T (solid) and water vapor K^ω (dashed) kernels under total sky conditions for the GFDL (red), the BMRC (blue) and the NCAR (green) models in units of W/m^2/K.

Figure 7: The global-mean water vapor, lapse-rate, water vapor+lapse rate, surface albedo and cloud feedbacks computed for 14 coupled ocean-atmosphere models (listed in Table 1 of Soden and Held, 2006) using the GFDL (red), NCAR (green), BMRC (blue) kernels. The global-mean change in cloud radiative forcing per degree global warming (black dots) and the adjusted change in cloud radiative forcing based on each of the three kernels are also shown. Only 12 of the 14 models archived the necessary data for computing cloud feedbacks and only 11 of the 14 archived the necessary data for computing the change in cloud radiative forcing.

Figure 8: Multi-model ensemble-mean maps of the temperature, water vapor, albedo and cloud feedback computed using climate response patterns from the IPCC AR4 models and the GFDL radiative kernels.

Figure 9: Same as figure 11, only for the clear-sky feedbacks.

Figure 10: Multi-model ensemble-mean maps of the corrections to dC_{RF} for temperature (top left), water vapor (top right), surface albedo (lower left), and their sum (lower right) computed using climate response patterns from the IPCC AR4 models and the GFDL radiative kernels.

Figure 11: Multi-model ensemble-mean maps of the cloud feedback estimated as the residual of the kernel calculations (top), the change in cloud forcing (middle), and the change in cloud

forcing after adjusting for the effects of cloud masking on non-cloud feedbacks and external radiative forcing (bottom). Only those models for which both the cloud feedback and cloud radiative forcing were available are included in the ensemble mean. Both the cloud feedback and cloud masking adjustments to the change in cloud forcing are estimated using the GFDL kernel.

Figures

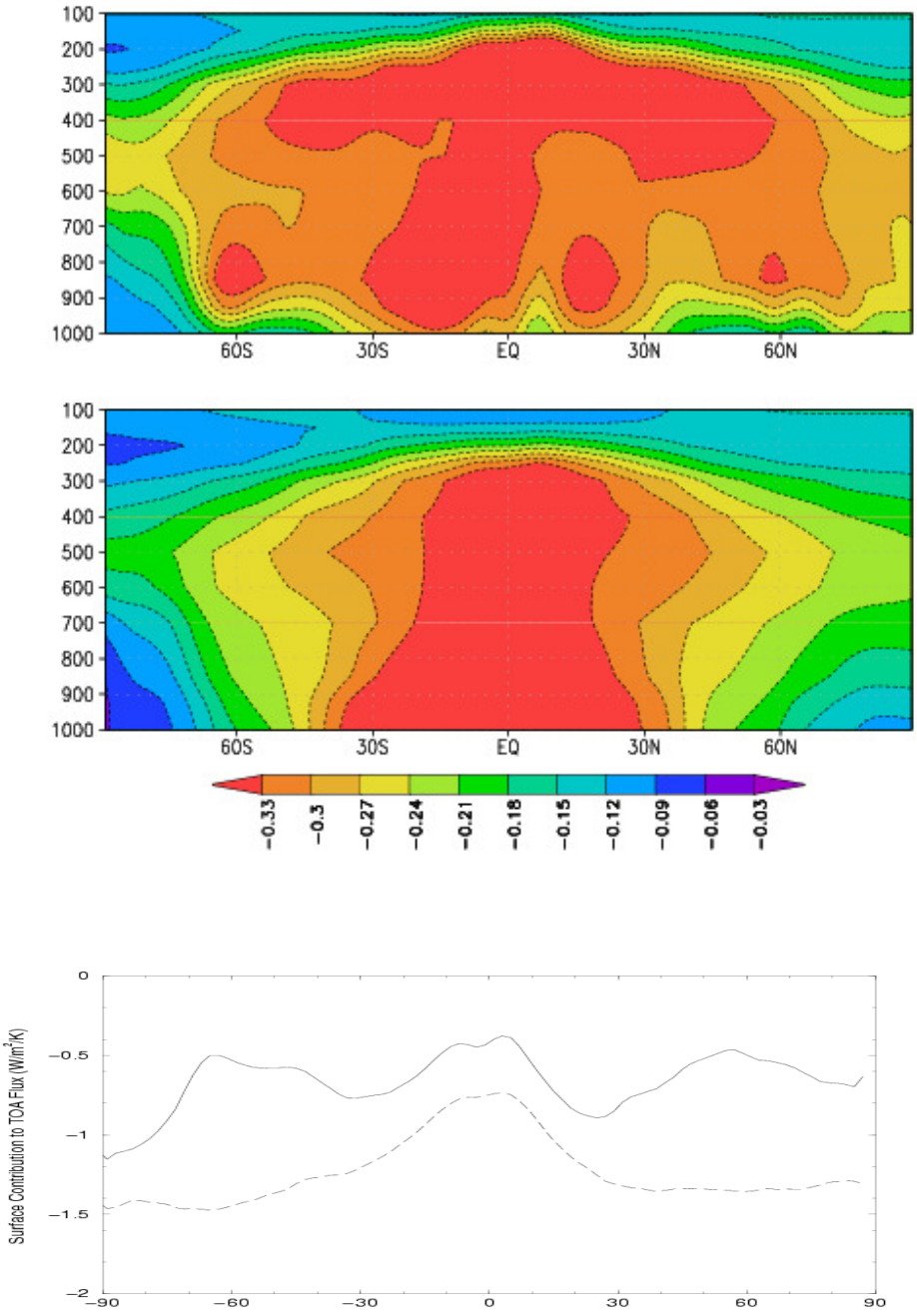

Figure 1 The zonal-mean, annual-mean temperature kernel K^T under total sky (top) and clear sky (middle) conditions in units of W/m^2/K/100hPa. The surface component of the kernel is shown separately (bottom) for both total-sky (solid) and clear-sky (dashed).

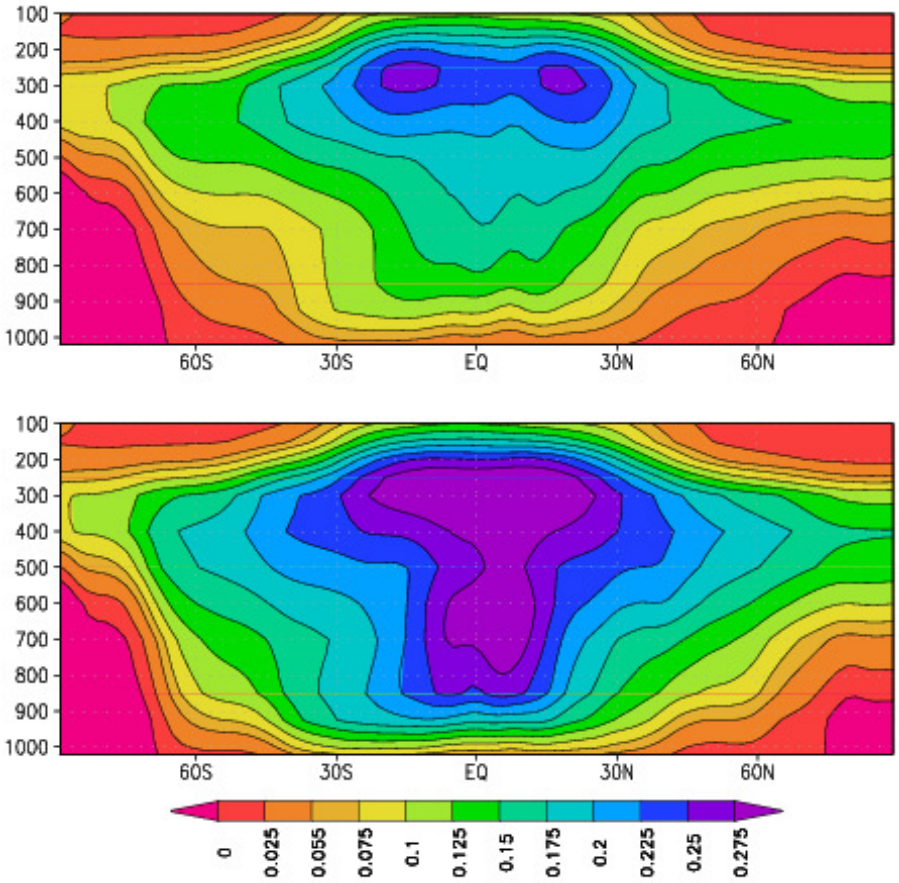

Figure 2 The zonal-mean, annual-mean water vapor kernel K^{ω} under total sky (top) and clear sky (bottom) conditions in units of W/m^2/K/100hPa. When multiplied by the vapor response (1 unit of vapor is required to maintain constant relative humidity for a 1K temperature increase), a pressure average of K^{ω} yields the total effect of the column temperature perturbation on the TOA longwave flux.

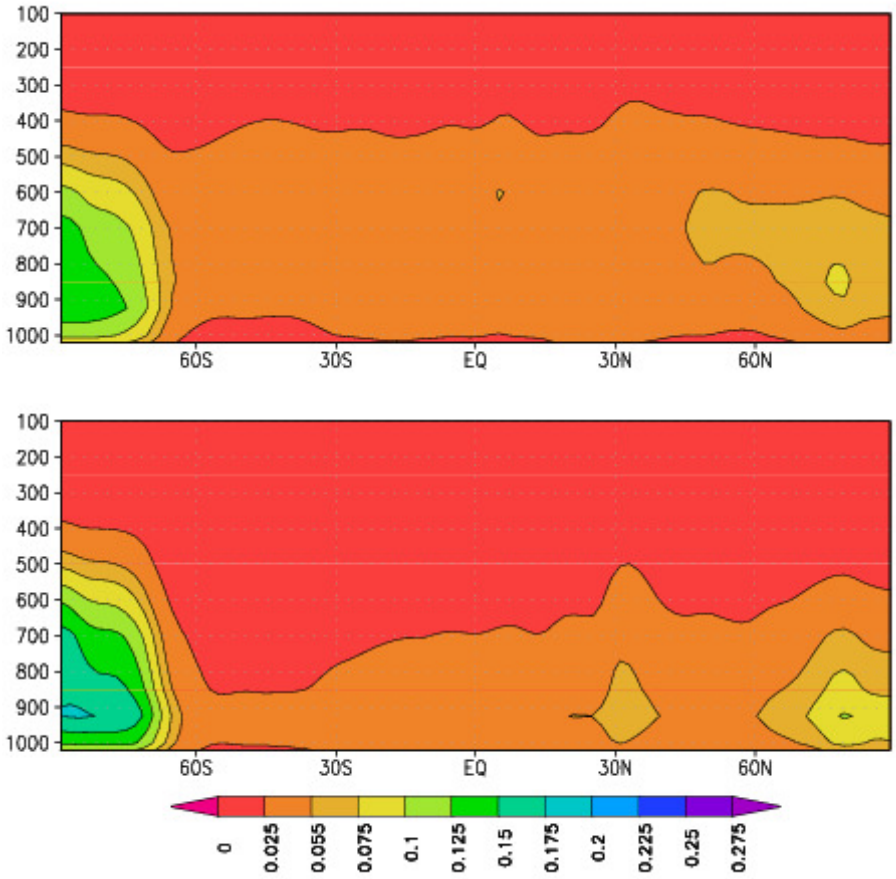

Figure 3 Same as figure 2, but for the net downward shortwave radiation at the TOA.

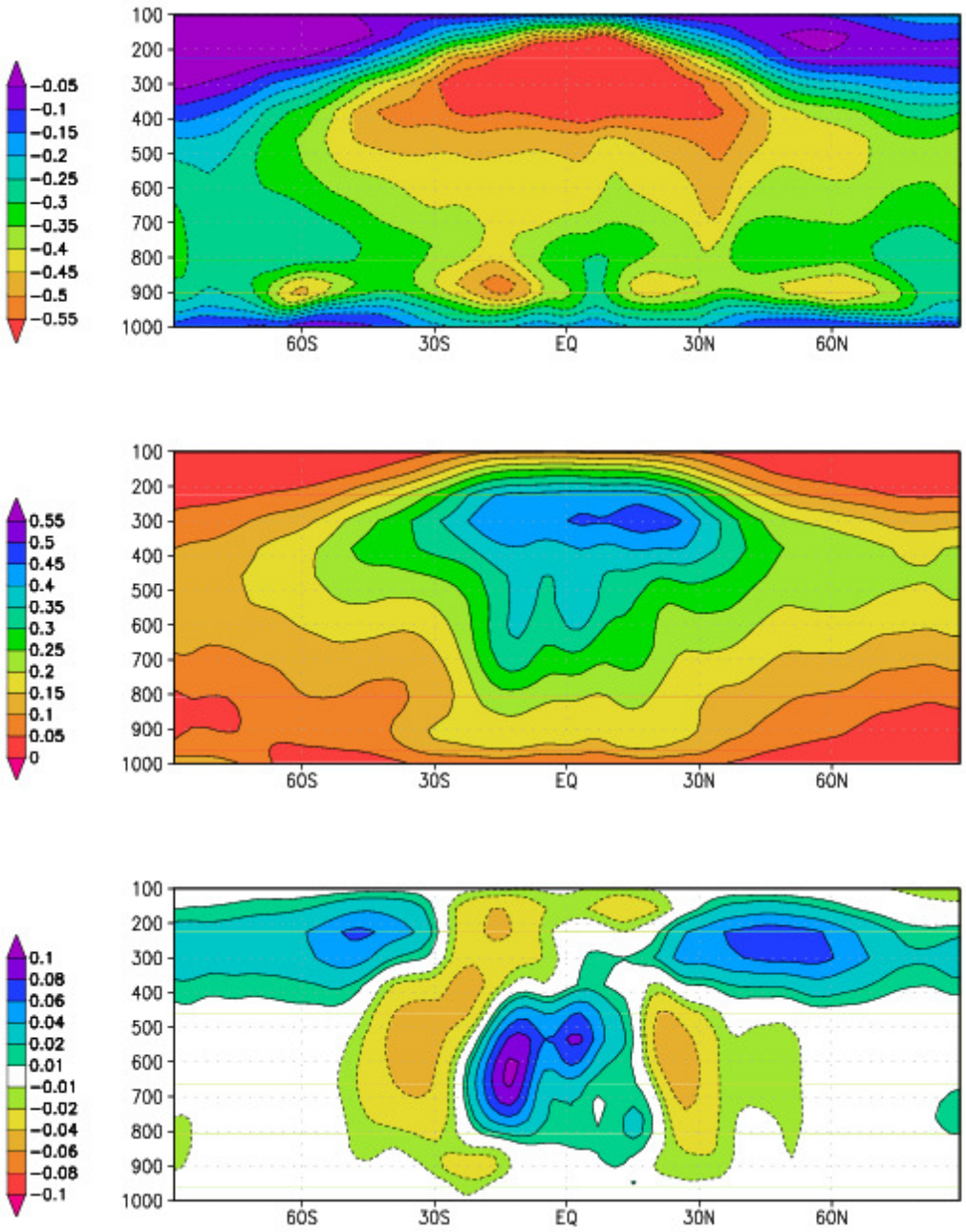

Figure 4 The total-sky TOA flux response due to the temperature perturbations (top) and water vapor (middle) displayed in Fig. 5. The bottom plot shows the portion of the water vapor effect that is due to departures from constant relative humidity. Positive values indicate an increase in net outgoing radiation (i.e., a cooling effect). The results are normalized by the change in global mean surface temperature and are expressed in units of W/m^2/K/100hPa.

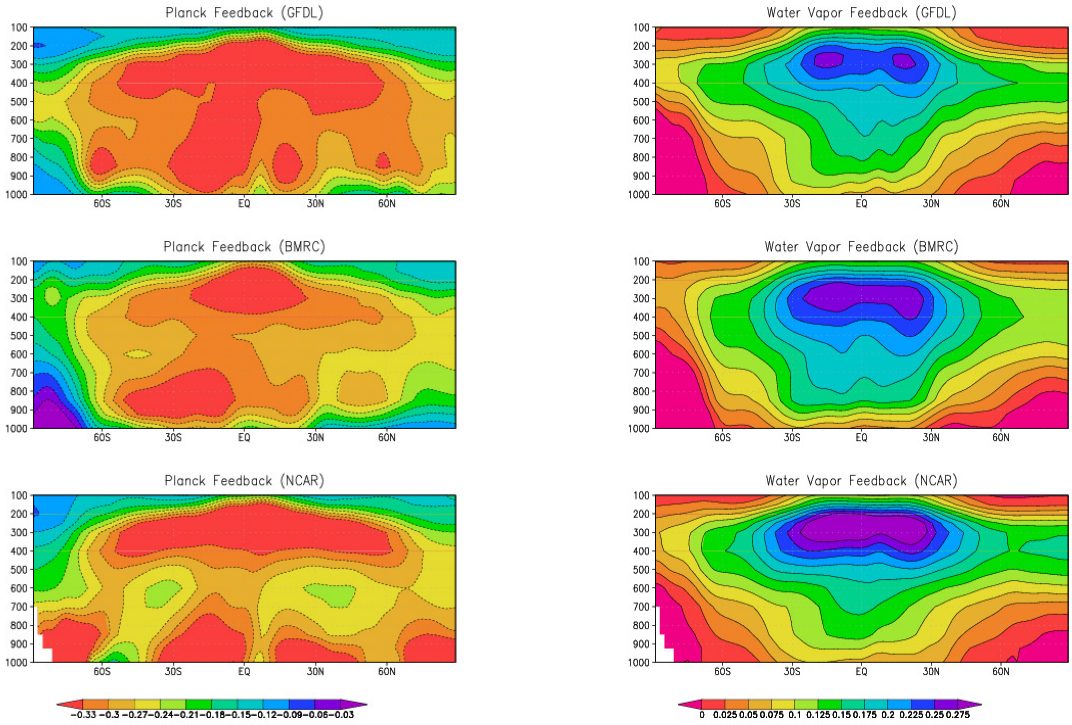

Figure 5: The annual-mean, zonal-mean temperature K^T and water vapor K^ω kernels under total sky conditions for the GFDL (top), BMRC (middle) and NCAR (bottom) models in units of W/m^2/K/100hPa.

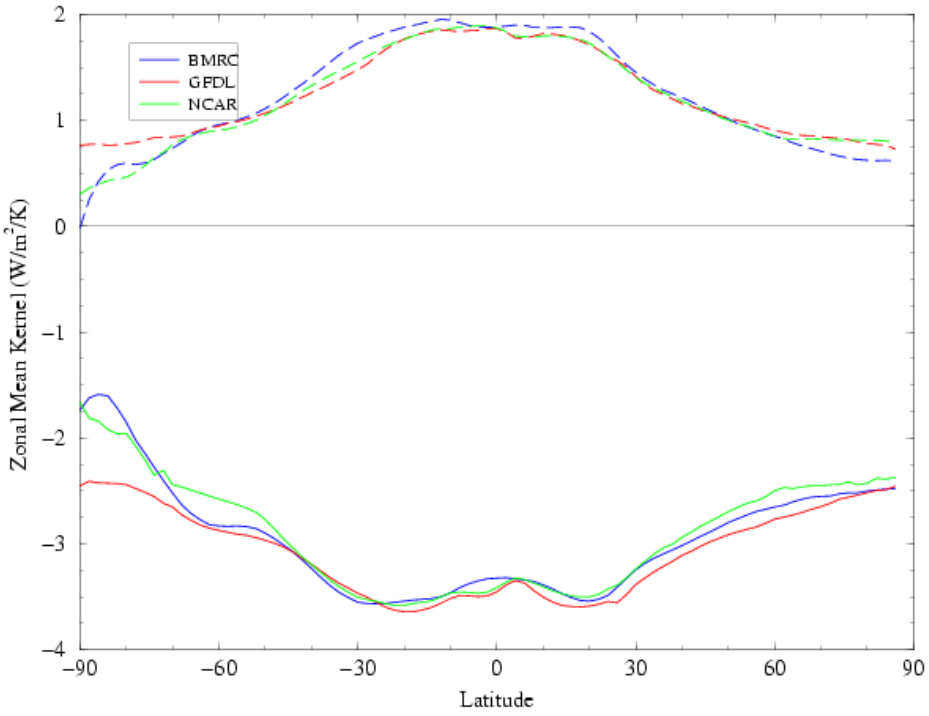

Figure 6: Zonal, annual-mean of the vertically-integrated temperature K^T (solid) and water vapor K^ω (dashed) kernels under total sky conditions for the GFDL (red), the BMRC (blue) and the NCAR (green) models in units of W/m^2/K.

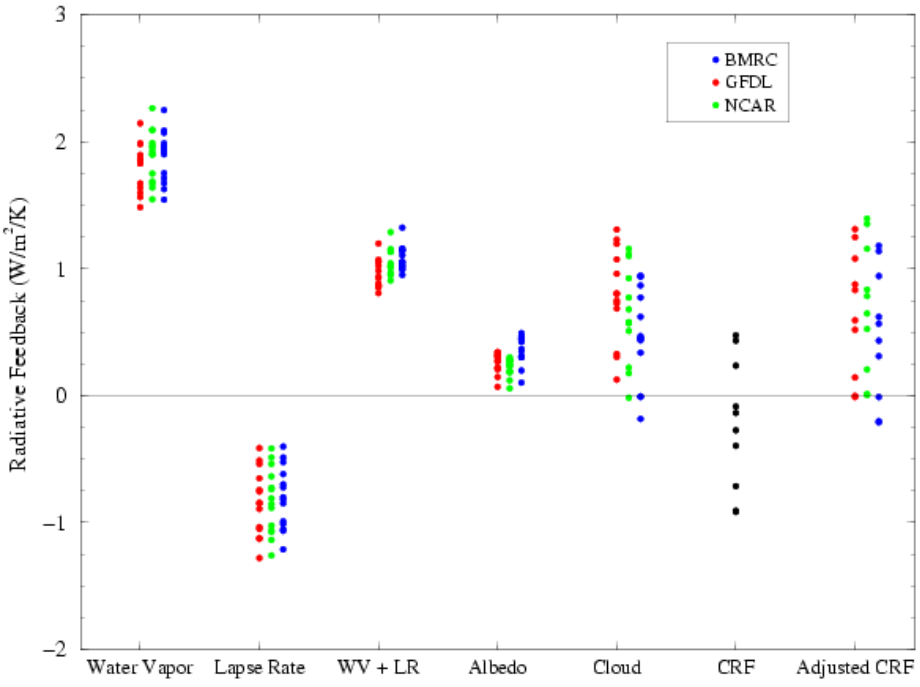

Figure 7: The global-mean water vapor, lapse-rate, water vapor+lapse rate, surface albedo and cloud feedbacks computed for 14 coupled ocean-atmosphere models (listed in Table 1 of Soden and Held, 2006) using the GFDL (red), NCAR (green), BMRC (blue) kernels. The global-mean change in cloud radiative forcing per degree global warming (black dots) and the adjusted change in cloud radiative forcing based on each of the three kernels are also shown. Only 12 of the 14 models archived the necessary data for computing cloud feedbacks and only 11 of the 14 archived the necessary data for computing the change in cloud radiative forcing.

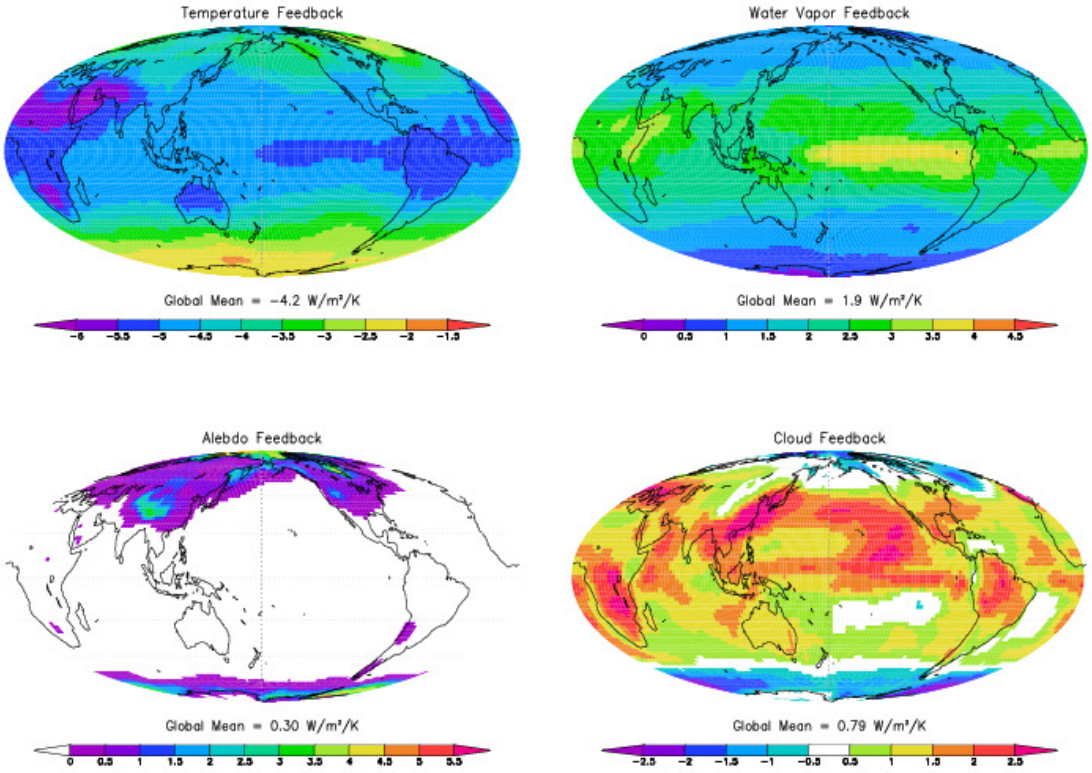

Figure 8: Multi-model ensemble-mean maps of the temperature, water vapor, albedo and cloud feedback computed using climate response patterns from the IPCC AR4 models and the GFDL radiative kernels.

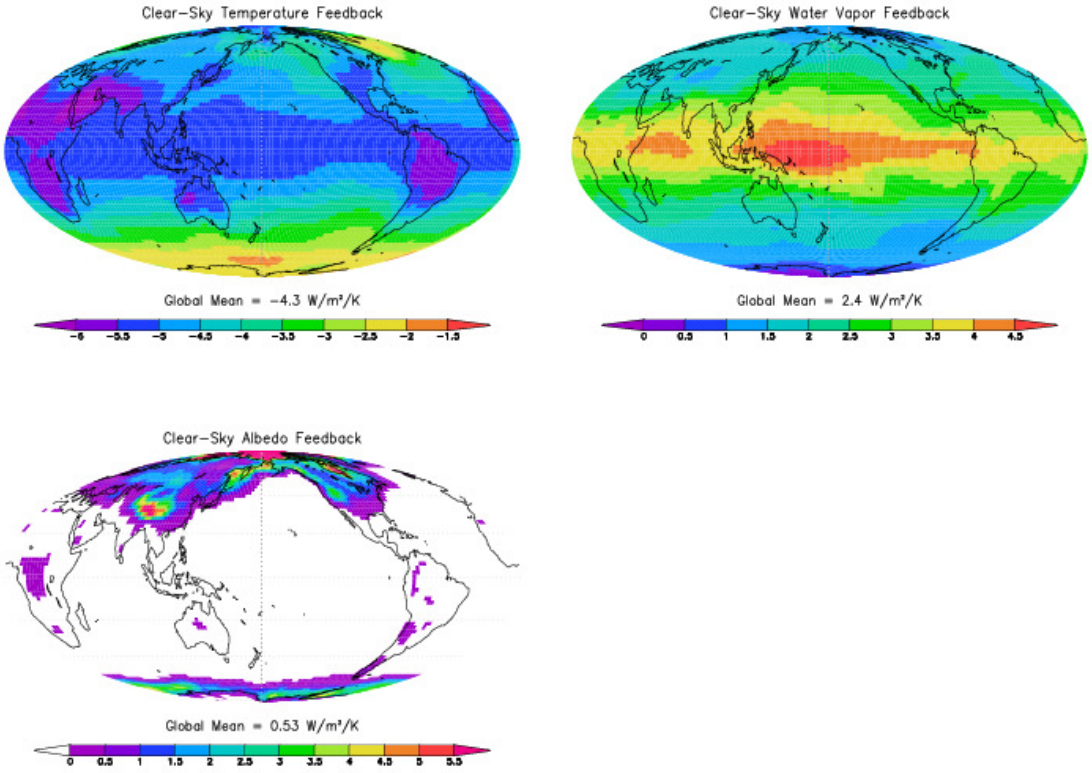

Figure 9: Same as figure 11, only for the clear-sky feedbacks.

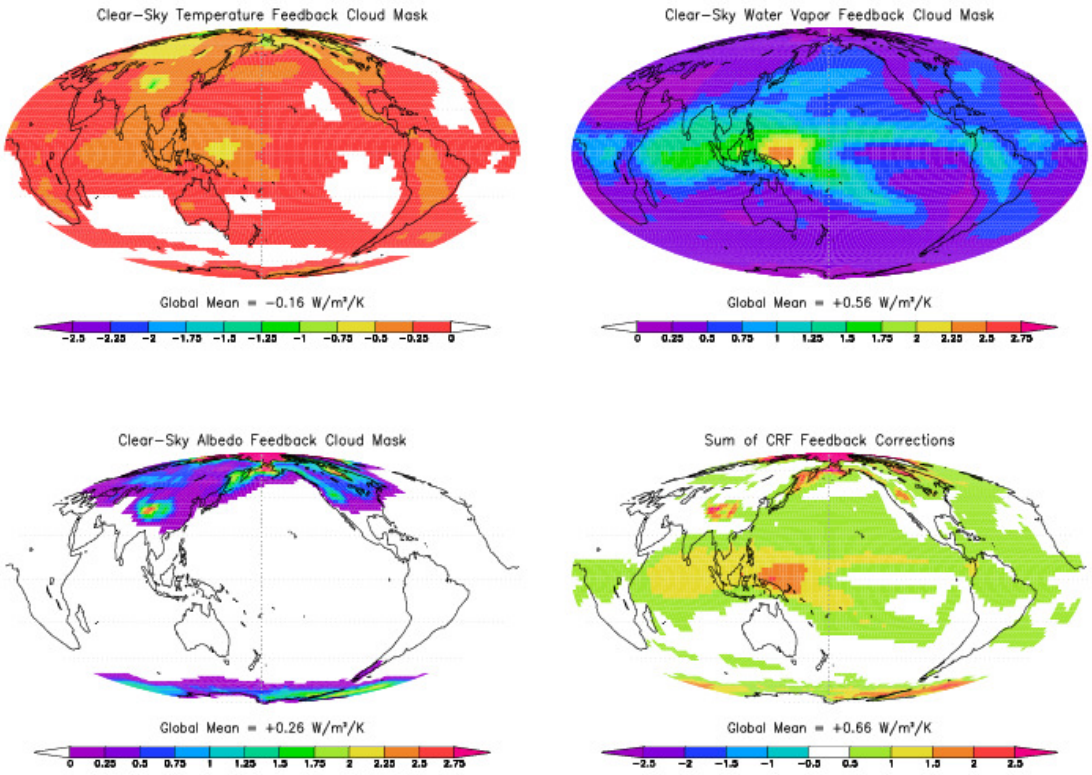

Figure 10: Multi-model ensemble-mean maps of the corrections to dC_{RF} for temperature (top left), water vapor (top right), surface albedo (lower left), and their sum (lower right) computed using climate response patterns from the IPCC AR4 models and the GFDL radiative kernels.

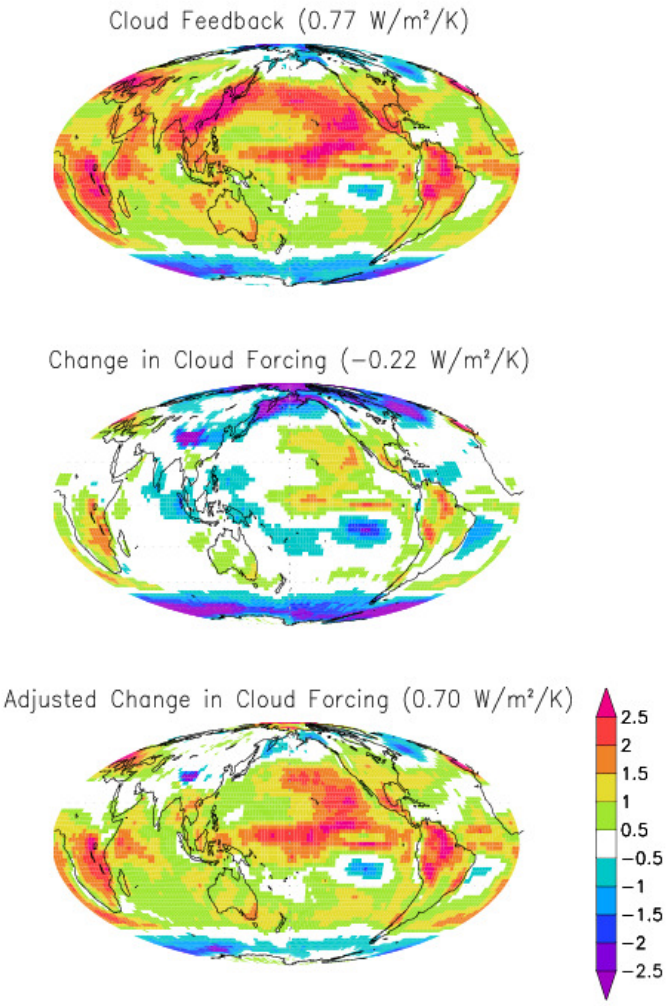

Figure 11: Multi-model ensemble-mean maps of the cloud feedback estimated as the residual of the kernel calculations (top), the change in cloud forcing (middle), and the change in cloud forcing after adjusting for the effects of cloud masking on non-cloud feedbacks and external radiative forcing (bottom). Only those models for which both the cloud feedback and cloud radiative forcing were available are included in the ensemble mean. Both the cloud feedback and cloud masking adjustments to the change in cloud forcing are estimated using the GFDL kernel.

	Temperature	Water Vapor (LW)	Water Vapor (SW)
Total Sky	**-3.25**	**1.13**	**0.27**
Clear Sky	**-3.56**	**1.62**	**0.16**

Table 1: The global-mean vertically-integrated values of the temperature and water vapor kernels for total-sky and clear-sky conditions. The kernels are integrated from surface to the tropopause and the results are expressed in units of $W/m^2/K$.

Feedback	Kernel	Forward PRP	Reverse PRP	Average PRP
Temperature	**-4.06**	-4.42	-3.64	**-4.03**
Water Vapor	**2.01**	2.12	1.78	**1.95**
Surface Albedo	**0.15**	0.17	0.13	**0.15**
Clouds	**0.37**	0.28	0.39	**0.34**

Table 2: Comparison feedback calculations using the PRP method and kernel method for the GFDL AM2 under a +2/-2 K SST perturbation. All values are in units of $W/m^2/K$.

Model	Temperature	Water Vapor LW	Water Vapor SW	Sfc Albedo
GFDL	-3.25 (-3.56)	1.13 (1.62)	0.27 (0.16)	1.39 (2.11)
NCAR	-3.13 (-3.52)	1.19 (1.68)	0.23 (0.15)	1.35 (2.13)
BMRC (FS/LH)	-3.17 (-3.58)	1.25 (1.76)	0.23 (0.17)	1.56 (2.22)
BMRC (SES)	-3.14	1.35	0.26	1.61

Table 3: Global-mean vertical integrals from surface to the tropopause of the temperature and water vapor feedback kernels in units of $W/m^2/K$. For surface albedo, the units are W/m2/ per 1% decrease in surface albedo. The corresponding integrals for the clear-sky kernels are listed in parentheses.